BENTHAM SCIENCE

CrossMark

# Current Medical Imaging

Content list available at: https://benthamscience.com/journals/cmir

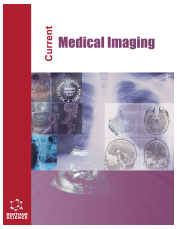


RESEARCH ARTICLE

# Comparison between Conventional Breath-hold and Respiratory-triggered Magnetic Resonance Cholangiopancreatography with and without Compressed Sensing: Cross-sectional Study

Younguk Kim[1], Eun Sun Lee[1,*], Hyun Jeong Park[1], Sung Bin Park[1], Bernd Kuehn[2], Jae Kon Sung[3], Yaeji Lim[4] and Changwoo Kim[4]

[1]*Department of Radiology, Chung-Ang University Hospital 102, Heukseok-ro, Dongjak-gu, Seoul 06973, Republic of Korea*
[2]*Department of MR Engineering, Siemens Healthcare GmbH, Henkestr 127, Erlangen 91052, Germany*
[3]*Department of MR Engineering, Siemens Healthineers Ltd. 23, Chungjeong-ro, Seodaemun-gu, Seoul 03737, Republic of Korea*
[4]*Department of Applied Statistics, Chung-Ang University 102, Heukseok-ro, Dongjak-gu, Seoul 06973, Republic of Korea*

**Abstract:**

***Introduction:***

The application of compressed sensing (CS) has enabled breath-hold 3D-MRCP with a shorter acquisition time in clinical practice.

***Aim:***

To compare the image quality of breath-hold (BH) and respiratory-triggered (RT) 3D-MRCP with or without CS application in the same study population.

***Methods:***

In this retrospective study, from February to July 2020, a total of 98 consecutive patients underwent four different acquisition types of 3D-MRCP.; 1) BH MRCP with the generalized autocalibrating partially parallel acquisition (GRAPPA) (BH-GRAPPA), 2) RT-GRAPPA-MRCP, 3) RT-CS-MRCP and 4) BH-CS-MRCP. Relative contrast of common bile duct, 5-scale visibility score of biliary pancreatic ducts, 3-scale artifact score and 5-scale overall image quality score were evaluated by two abdominal radiologists.

***Results:***

Relative contrast value was significantly higher in BH-CS or RT-CS than in RT-GRAPPA (0.90 ± 0.057 and 0.89 ± 0.079, respectively, *vs*. 0.82 ± 0.071, $p < 0.01$) or BH-GRAPPA (*vs*. 0.77 ± 0.080, $p < 0.01$). The area affected by artifact was significantly lower in BH-CS among 4 MRCPs ($p < 0.01$). Overall image quality score in BH-CS was significantly higher than BH-GRAPPA (3.40 *vs*. 2.71, $p < 0.01$). There were no significant differences between RT-GRAPPA and BH-CS (*vs*. 3.13, $p = 0.67$) in overall image quality.

***Conclusion:***

In this study, our results revealed BH-CS had higher relative contrast and comparable or superior image quality among four MRCP sequences.

**Keywords:** Cholangiopancreatography, Magnetic resonance, Data compression, Image enhancement, Breath holding, Respiratory-gated imaging techniques.

| Article History | Received: August 31, 2022 | Revised: January 17, 2023 | Accepted: February 01, 2023 |
|---|---|---|---|

## 1. INTRODUCTION

Magnetic resonance cholangiopancreatography (MRCP) is a non-invasive imaging technique that provides detailed information on the anatomy and pathology of the pancreaticobiliary tract [1 - 3]. Although breath-hold (BH) two-dimensional thick-slab MRCP imaging is still the most commonly used MRCP technique, there have been recent advantages in three-dimensional (3D)-MRCP techniques, providing better visibility of the anatomy, a greater volume of coverage, thinner sections without inter-slice gaps, and higher signal-to-noise ratio [4 - 6].

* Address correspondende to this author at the Department of Radiology, Chung-Ang University Hospital, Chung-Ang University College of Medicine 102, Heukseok-ro, Dongjak-gu, Seoul 06973, Korea; Tel: 82-2-6299-3209; Fax: 82-2-6299-2017; E-mail: seraph377@gmail.com

However, since most 3D-MRCP sequences are performed in a respiratory-triggered (RT) manner, their acquisition time accounts for a significant portion of the total examination time, requiring up to 10 minutes or more, especially in patients with irregular respiration [7]. Furthermore, irregular breathing and long acquisition time render 3D-MRCP images prone to blurring and motion artifacts, often resulting in sub-optimal image quality [8].

Compressed sensing (CS), as one of the many efforts to reduce the acquisition time of 3D-MRCP, exploits the data sparsity and coded nature of magnetic resonance imaging (MRI) acquisition and enables accelerated MRI acquisition *via* an under-sampling of the k-space [4, 9 - 11]. The CS approach measures a relatively small number of random linear combinations of the signal values and then reconstructs the under-sampled data using a nonlinear optimization method [4, 12]. The application of CS has enabled BH-3D-MRCP and RT-3D-MRCP with a shorter acquisition time in clinical practice [4, 7, 13, 14].

Previous studies have demonstrated the feasibility of BH-CS-MRCP and RT-CS-MRCP, as well as their similar or better image quality, while dramatically reducing the acquisition time, compared to that with conventional RT-3D-MRCP [4, 7, 13 - 16]. However, few studies have compared BH-3D-MRCP and RT 3D-MRCP with and without the application of CS in the same study samples. Therefore, the purpose of this study was to compare the image quality of these four 3D-MRCP sequences under the same study conditions.

## 2. MATERIALS AND METHODS

### 2.1. Study Population

This retrospective study was approved by our institutional review board (IRB No. 2107-025-19375), and the requirement of informed consent was waived. From February to July 2020, a total of 100 consecutive patients underwent MRCP. Indications for MRCP were as follows: pancreatic cystic lesions (n=23), common bile duct (CBD) stone assessment (n=21), bile ductal dilatation (n=12), pancreatic mass (n=12), acute pancreatitis (n=6), laboratory test abnormality (n=6), post-pancreaticoduodenectomy status (n=5), acute cholangitis (n=2), CBD mass (n=2), gallbladder cancer (n=2), perihilar mass (n=2), and etc. (n=7). The exclusion criterion was a failure to obtain the expected MRCP sequences (n=2), as shown in Fig. (**1**). Finally, 98 patients (54 men and 44 women; mean age, 63.2 years; age range, 16-84 years) were included in the quantitative and qualitative analyses.

### 2.2. MR Imaging Protocol

Two 3T MR systems (MAGNETOM Skyra, Siemens Healthcare, Erlangen, Germany), with an 18-channel body matrix coil combined with a 32-channel spine matrix coil, were used to obtain MRCP images.

Each patient underwent 3D-MRCP with four different acquisition sequences as follows: 1) BH-3D-MRCP based on sampling perfection with application-optimized contrasts using different flip-angle evolutions (SPACE), with the generalized autocalibrating partially parallel acquisition (GRAPPA) (BH-GRAPPA); 2) RT-3D-SPACE-GRAPPA-MRCP (RT-GRAPPA); 3) RT-CS-3D-SPACE-MRCP (RT-CS); and 4) BH-CS-3D-SPACE-MRCP (BH-CS). The detailed parameters are summarized in Table **1**. The acquisition order of the four MRCP sequences was random for each patient. For RT-MRCPs, the navigator-triggered prospective acquisition correction (PACE) technique was used [17].

### 2.3. Quantitative Image Analysis

A radiology resident with two years of experience who was blind to the patients' clinical information and MRCP protocol performed the quantitative image analysis. The obtained MRCP image was evaluated in the form of a maximum intensity projection (MIP). The mean signal intensity (SI) of the CBD ($SI_{CBD}$) was measured by placing a circular region of interest (ROI) on the CBD (Fig. **2**). The SI of the background ($SI_{background}$) was measured by placing an ROI on the most homogeneous part of the periductal background. Pancreaticobiliary ducts other than CBD were not included in the evaluation because they were too small to place the ROI.

**Table 1. Detailed parameters of four different sequences of the MRCPs.**

| - | RT-GRAPPA | RT-CS | BH-GRAPPA | BH-CS |
|---|---|---|---|---|
| FOV ($mm^2$) | 350×214 | 350×219 | 350×214 | 350×214 |
| TR (ms) | [a] | [a] | 2300 | 1700 |
| TE (ms) | 701 | 701 | 700 | 492 |
| FA (°) | 115 | 120 | 100 | 110 |
| Matrix | 320×205 | 384×250 | 320×95 | 320×150 |
| Acquisition plane | Coronal | Coronal | Coronal | Coronal |
| In-plane (interpolated) resolution (mm) | 1.0×1.0 (0.5×0.5) | 1.0×1.0 (0.5×0.5) | 1.0×1.0 (0.5×0.5) | 1.0×1.0 (0.5×0.5) |
| Slice thickness (mm) | 0.8 | 0.8 | 1.2 | 0.8 |
| Slice number | 120 | 120 | 72 | 120 |
| Fat suppression | SPAIR | SPAIR | SPAIR | SPAIR |
| Acceleration mode | GRAPPA | CS | GRAPPA | CS |
| Acceleration factor | 4 | 14 | 4 | 14 |
| Regularization parameter | - | 0.002 | - | 0.004 |
| Iteration | - | 20 | - | 20 |

*(Table 1) contd.....*

| - | RT-GRAPPA | RT-CS | BH-GRAPPA | BH-CS |
|---|---|---|---|---|
| NEX | 2 | 2 | 1.4 | 2 |
| Acquisition time (minute:second) | 3:32[a] | 1:51[a] | 0:21 | 0:16 |

**Note:**[a]Variable depending on the patient's respiratory rate

MRCP: magnetic resonance cholangiopancreatography, RT: respiratory-triggered; BH: breath hold, CS: compressed sensing, GRAPPA: generalized autocalibrating partially parallel acquisition, FOV: field of view, TR: repetition time, TE: echo time, FA: flip angle, PAT: parallel imaging technique, SPAIR: spectral attenuated inversion recovery, NEX: number of excitations

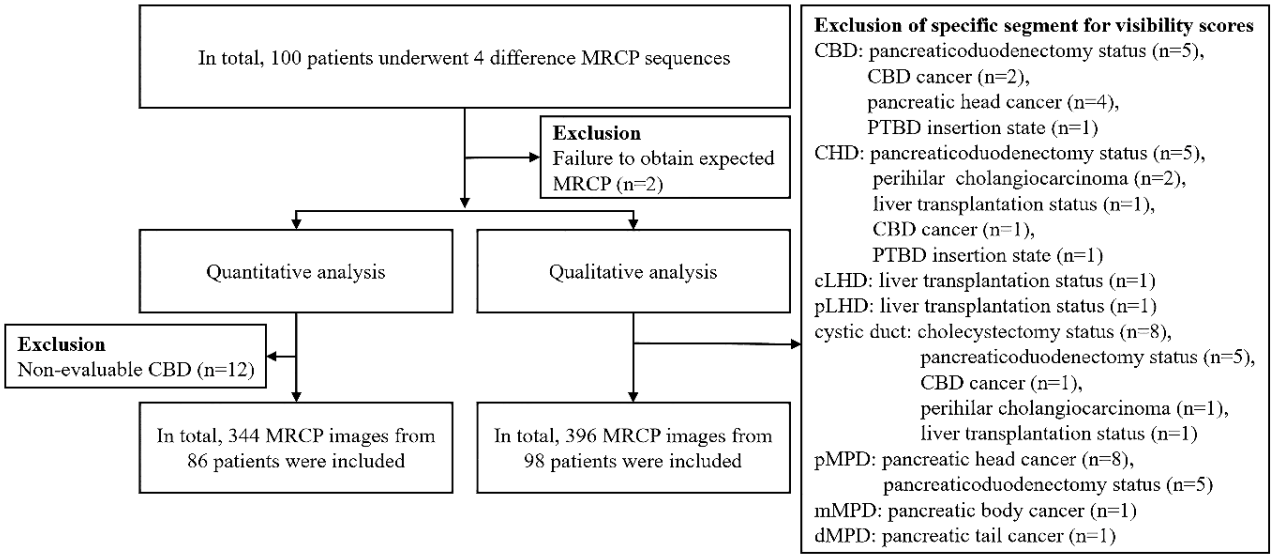


**Fig. (1).** Flow diagram showing the number of patients and reasons for exclusion.

**Note**: *CBD: common bile duct, CHD: common hepatic duct, cRHD: central right hepatic duct, pRHD: peripheral right hepatic duct, cLHD: central left hepatic duct, pLHD: peripheral left hepatic duct, pMPD: proximal main pancreatic duct, mMPD: middle main pancreatic duct, dMPD: distal main pancreatic duct, PTBD: percutaneous transhepatic biliary drainage.*

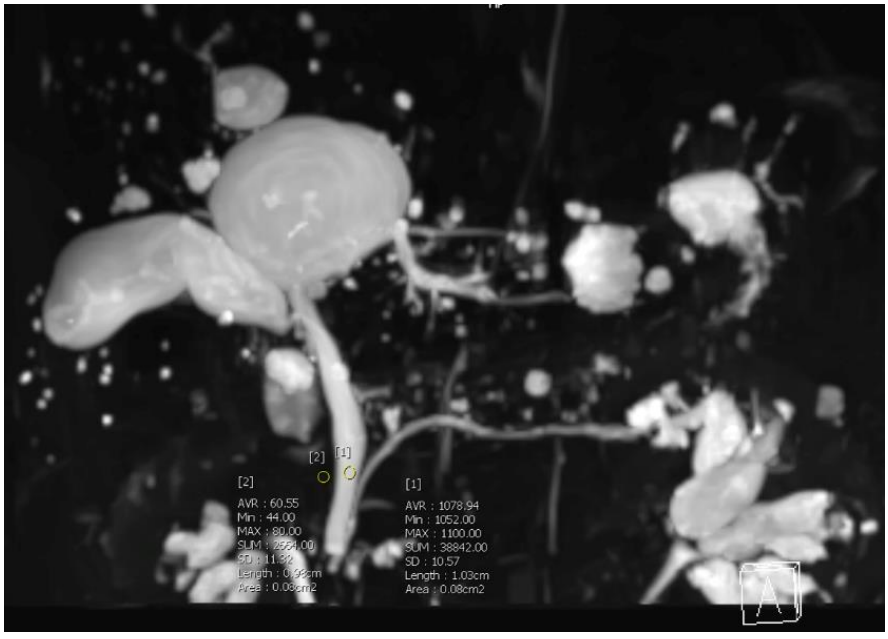


**Fig. (2).** An example of placing region of interests (ROIs).

The relative contrast (RC) was calculated by placing ROIs on the common bile duct and background parenchyma.

**Note**: *AVR: average signal intensity; SD, standard deviation.*

For images acquired using an undersampling method such as CS, conventional methods of SNR calculation may be unreliable due to the heterogeneous signal intensity of the background [4, 18]. Therefore, for each MRCP sequence, we calculated the relative contrast (RC) between the CBD and background as $(SI_{CBD} - SI_{background})/(SI_{CBD} + SI_{background})$ [18]. The RC was measured three times repeatedly on a MIP image of MRCP sequences and the average was used for analysis.

If the CBD was not visible, possibly due to previous surgery or replacing mass, the RC was treated as non-evaluable. At the data processing step, if the RC value of any of the four sequences for one patient was non-evaluable, all MRCP data of that patient were excluded from quantitative analysis (n=12). In total, 344 MRCP images from 86 patients were included in the quantitative analysis, as shown in Fig. (**1**).

### 2.4. Qualitative Image Analysis

Two board-certificated abdominal radiologists with 16 years of experience (L.E.S. and P.H.J.) who were blind to the patient's clinical information and MRCP protocol performed the qualitative analysis. MIP images of the MRCP were also used for evaluation. The readers evaluated ductal visibility, artifact degree, and overall image quality for each MRCP image. The detailed scoring systems are tabulated in Table **2**. The higher scores meant that ducts were well visualized, there were few areas affected by artifacts, and overall image quality was better.

For the visibility score, we divided the pancreati cobiliary duct into the following 10 segments. – 1) CBD, 2) common hepatic duct [CHD], 3) central right hepatic duct [cRHD], 4) peripheral right hepatic duct [pRHD], 5) central left hepatic duct [cLHD], 6) peripheral left hepatic duct [pLHD], 7) cystic duct, 8) proximal MPD [pMPD], 9) middle MPD [mMPD] and 10) distal MPD [dMPD]. Central and peripheral hepatic ducts were divided based on the half point between CHD and the capsule of the liver, and MPD was equally divided into three segments. At the data processing step, some segments of the visibility score were treated as non-evaluable because of the patient's clinical history; detailed reasons are summarized in Fig. (**1**). Finally, a total of 396 MRCP images from 98 patients were included in the qualitative analysis.

### 2.5. Statistical Analysis

In the quantitative analysis, differences in RCs among BH-CS, RT-CS, BH-GRAPPA, and RT-GRAPPA were evaluated using the generalized estimating equations (GEE) model; if significant differences were found in the GEE model analysis, paired *t*-tests with Bonferroni correction were performed.

In the qualitative analysis, the Friedman test was used to evaluate differences in scores among the four MRCP sequences. Similarly, the Wilcoxon signed-rank test with Bonferroni correction was used for pairwise comparisons. The agreement between observers in scores was evaluated using Cohen's weighted kappa. $\kappa$ values $\leq 0$ were considered as indicating no agreement, 0.01 – 0.20 as none to slight, 0.21 – 0.40 as fair, 0.41 – 0.60 as moderate, 0.61 – 0.80 as substantial, and 0.81–1.00 as almost perfect agreement.

For all analyses, a $p$-value of <0.05 was considered significant, and for paired *t*-tests and Wilcoxon signed-rank tests, Bonferroni-corrected $p$-values were computed. All statistical analyses were performed by statisticians using R software (version 3.2.4; R Foundation for Statistical Computing, Vienna, Austria).

## 3. RESULTS

### 3.1. Quantitative Analysis

The RC values of the CBD in four MRCPs were visualized as box-plot (Fig. **3**). In the GEE model analysis, the RC of the CBD significantly differed among the sequences when using RT-GRAPPA as a reference (Table **3**). In paired *t*-tests with Bonferroni correction, the RC was significantly higher for BH-CS or RT-CS than for RT-GRAPPA (mean ± standard deviation: 0.90 ± 0.057 and 0.89 ± 0.079, respectively *vs*. 0.82 ± 0.071, $p < 0.01$) or BH-GRAPPA (*vs*. 0.77 ± 0.080, $p < 0.01$). Additionally, the RC was significantly higher for RT-GRAPPA than for BH-GRAPPA ($p < 0.01$). There was no significant difference between BH-CS and RT-CS ($p$=0.6).

**Table 2. Scoring system for qualitative evaluation.**

| Parameter | Scoring System |
|---|---|
| Ductal visibility | 5: excellent visualization of the segments with good sharpness and contrast against the surrounding structures<br>4: good visualization of the segments with some blurring<br>3: partial visualization of the segment<br>2: equivocal visualization with minimal contrast against the surrounding structures<br>1: poor visualization of the segments |
| Artifact | 3: minimal areas affected by motion artifact<br>2: partial areas affected by motion artifact<br>1: entire area affected by severe motion artifact |
| Overall image quality | 5: excellent image quality<br>4: good image quality<br>3: average image quality<br>2: poor image quality<br>1: non-diagnostic image quality |

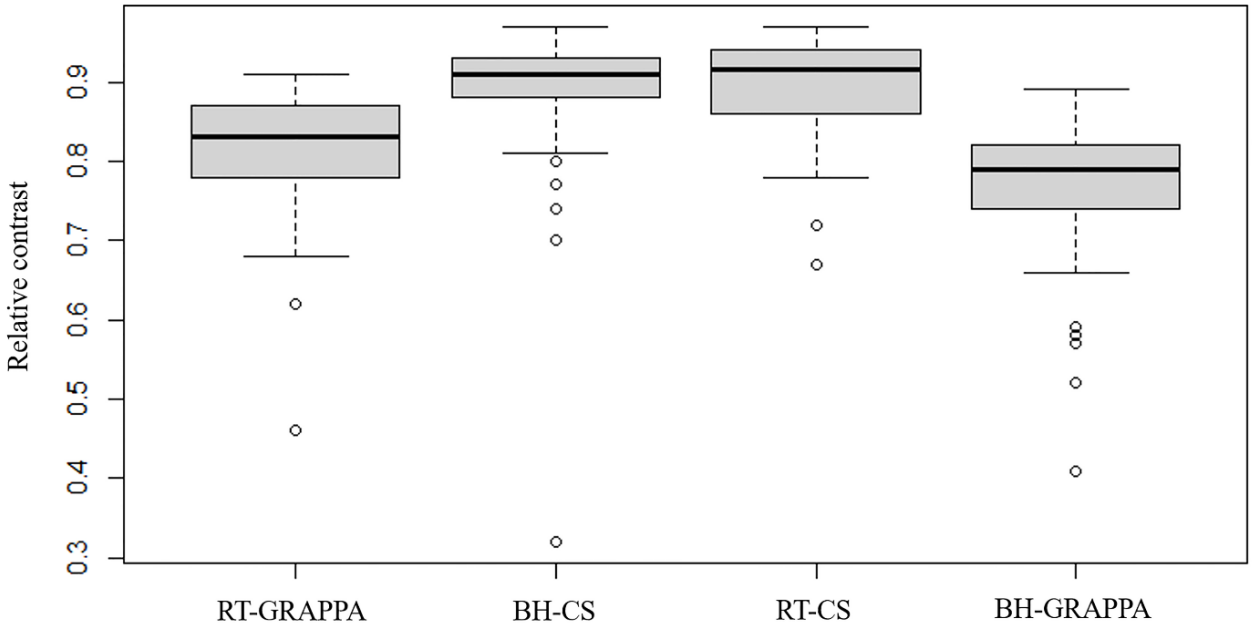


**Fig. (3).** Box plot of relative contrast of the common bile duct.
**Note**: *RT: respiratory-triggered; BH: breath hold, CS: compressed sensing, GRAPPA: generalized autocalibrating partially parallel acquisition.*

**Table 3. Quantitative analysis results of relative contrast.**

| - | - | **GEE model estimates** | |
|---|---|---|---|
| - | **Mean RC[a]** | **β(SE)[b]** | ***p*-value** |
| RT-GRAPPA | 0.082±0.071 | Reference | - |
| RT-CS | 0.90±0.057 | 0.086(0.011) | <0.01 |
| BH-GRAPPA | 0.77±0.080 | -0.042(0.007) | <0.01 |
| BH-CS | 0.89±0.079 | 0.080(0.011) | <0.01 |

**Note:** GEE: generalized estimating equations, SE: standard error, RC: relative contrast, RT: respiratory-triggered; BH: breath hold, CS: compressed sensing, GRAPPA: generalized autocalibrating partially parallel acquisition
[a] Data are mean±standard deviation
[b] Adjusted mean difference compared to the reference group

**Table 4. Scores of qualitative analysis in RT-GRAPPA, BH-GRAPPA, RT-CS and BH-CS sequences.**

| **Parameter** | **Reader** | **RT-GRAPPA** | **BH-GRAPPA** | **RT-CS** | **BH-CS** | ***κ* value** | ***p*-value** |
|---|---|---|---|---|---|---|---|
| Visibility | - | - | - | - | - | - | - |
| CBD | Reader1 | 4.20±0.84 | 4.16±0.81 | 4.31±0.88 | 4.55±0.57 | 0.84 | <0.01 |
| - | Reader2 | 4.22±0.86 | 4.10±0.78 | 4.26±0.91 | 4.49±0.59 | - | <0.01 |
| CHD | Reader1 | 4.23±0.75 | 4.20±0.80 | 4.42±0.66 | 4.57±0.60 | 0.71 | <0.01 |
| - | Reader2 | 4.05±0.88 | 3.97±0.86 | 4.27±0.78 | 4.41±0.67 | - | <0.01 |
| cRHD | Reader1 | 3.76±1.11 | 3.53±0.97 | 3.88±1.00 | 3.99±0.94 | 0.91 | <0.01 |
| - | Reader2 | 3.76±1.07 | 3.54±0.92 | 3.85±0.97 | 3.96±0.88 | - | <0.01 |
| pRHD | Reader1 | 3.05±1.34 | 2.61±1.22 | 2.99±1.21 | 2.85±1.26 | 0.93 | <0.01 |
| - | Reader2 | 3.02±1.27 | 2.56±1.16 | 2.94±1.21 | 2.91±1.22 | - | <0.01 |
| cLHD | Reader1 | 3.73±1.06 | 3.52±0.89 | 3.82±1.00 | 3.98±0.91 | 0.89 | <0.01 |
| - | Reader2 | 3.67±1.10 | 3.38±0.92 | 3.71±1.07 | 3.90±0.86 | - | <0.01 |
| pLHD | Reader1 | 2.73±1.18 | 2.22±1.09 | 2.67±1.06 | 2.58±1.08 | 0.93 | <0.01 |
| - | Reader2 | 2.74±1.22 | 2.23±1.08 | 2.66±1.10 | 2.59±1.06 | - | <0.01 |
| Cystic duct | Reader1 | 3.26±1.08 | 3.23±1.11 | 3.54±1.06 | 3.78±1.09 | 0.80 | <0.01 |
| - | Reader2 | 3.23±1.00 | 3.16±1.06 | 3.51±1.09 | 3.61±1.00 | - | <0.01 |

*(Table 4) contd.....*

| Parameter | Reader | RT-GRAPPA | BH-GRAPPA | RT-CS | BH-CS | $\kappa$ value | *p*-value |
|---|---|---|---|---|---|---|---|
| pMPD | Reader1 | 3.73±1.11 | 3.39±1.11 | 3.84±1.23 | 3.87±1.15 | 0.82 | <0.01 |
| - | Reader2 | 3.69±1.04 | 3.34±1.12 | 3.69±1.21 | 3.74±1.11 | - | <0.01 |
| mMPD | Reader1 | 3.68±1.00 | 3.03±1.16 | 3.59±1.16 | 3.62±1.23 | 0.80 | <0.01 |
| - | Reader2 | 3.43±1.03 | 3.01±1.15 | 3.55±1.15 | 3.38±1.15 | - | <0.01 |
| dMPD | Reader1 | 3.10±1.19 | 2.66±1.23 | 3.19±1.24 | 2.96±1.31 | 0.85 | <0.01 |
| - | Reader2 | 3.04±1.10 | 2.58±1.20 | 3.11±1.16 | 2.80±1.18 | - | <0.01 |
| Artifact | Reader1 | 2.18±0.72 | 1.84±0.57 | 2.16±0.78 | 2.64±0.58 | 0.88 | <0.01 |
| - | Reader2 | 2.20±0.70 | 1.86±0.57 | 2.18±0.79 | 2.57±0.61 | - | <0.01 |
| Overall image quality | Reader1 | 3.13±1.09 | 2.71±0.96 | 3.21±1.13 | 3.40±0.93 | 0.99 | <0.01 |
| | Reader2 | 3.14±1.10 | 2.71±0.97 | 3.24±1.16 | 3.40±0.93 | - | <0.01 |

**Note:** Data are mean ± 1 standard deviation. $\kappa$ values are for Cohen's weighted kappa. *p*-values are for Friedman test CBD common bile duct, CHD common hepatic duct, cRHD central right hepatic duct, pRHD peripheral right hepatic duct, cLHD central left hepatic duct, pLHD peripheral left hepatic duct, pMPD proximal main pancreatic duct, mMPD middle main pancreatic duct, dMPD distal main pancreatic duct

**Table 5. Pairwise comparison of RT-GRAPPA, BH-GRAPPA, RT-CS and BH-CS sequences.**

| - | - | RT-GRAPPA & RT-CS | RT-GRAPPA & BH-CS | RT-GRAPPA & BH-GRAPA | RT-CS & BH-CS | BH-GRAPPA & RT-CS | BH-GRAPPA & BH-CS |
|---|---|---|---|---|---|---|---|
| Visibility | - | - | - | - | - | - | - |
| CBD | Reader1 | 1.00 | **0.03*** | 1.00 | 0.87 | 0.47 | **<0.01*** |
| - | Reader2 | 1.00 | 0.40 | 0.96 | 1.00 | 0.41 | **<0.01*** |
| CHD | Reader1 | 0.46 | **<0.01*** | 1.00 | 0.60 | 0.39 | **<0.01*** |
| - | Reader2 | 0.50 | **0.03*** | 1.00 | 1.00 | 0.08 | **<0.01*** |
| cRHD | Reader1 | 1.00 | 1.00 | 0.35 | 1.00 | 0.10 | **0.01*** |
| - | Reader2 | 1.00 | 1.00 | 0.30 | 1.00 | 0.14 | **0.01*** |
| pRHD | Reader1 | 1.00 | 1.00 | 0.11 | 1.00 | 0.23 | 1.00 |
| - | Reader2 | 1.00 | 1.00 | 0.06 | 1.00 | 0.21 | 0.32 |
| cLHD | Reader1 | 1.00 | 0.78 | 0.37 | 1.00 | 0.13 | **<0.01*** |
| - | Reader2 | 1.00 | 1.00 | 0.11 | 1.00 | 0.07 | **<0.01*** |
| pLHD | Reader1 | 1.00 | 1.00 | **0.01*** | 1.00 | **0.02*** | 0.11 |
| - | Reader2 | 1.00 | 1.00 | **0.02*** | 1.00 | **0.04*** | 0.10 |
| Cystic duct | Reader1 | 0.57 | **0.01*** | 1.00 | 0.60 | 0.54 | **0.01*** |
| - | Reader2 | 0.58 | 0.06 | 1.00 | 1.00 | 0.31 | **0.02*** |
| pMPD | Reader1 | 1.00 | 1.00 | 0.16 | 1.00 | **0.01*** | **0.01*** |
| - | Reader2 | 1.00 | 1.00 | 0.23 | 1.00 | 0.13 | 0.06 |
| mMPD | Reader1 | 1.00 | 1.00 | **<0.01*** | 1.00 | **<0.01*** | **<0.01*** |
| - | Reader2 | 1.00 | 1.00 | 0.11 | 1.00 | **0.01*** | 0.17 |
| dMPD | Reader1 | 1.00 | 1.00 | 0.07 | 1.00 | **0.02*** | 0.81 |
| - | Reader2 | 1.00 | 0.89 | **0.04*** | 0.35 | **0.01*** | 1.00 |
| Artifact | Reader1 | 1.00 | **<0.01*** | **<0.01*** | **<0.01*** | **0.01*** | **<0.01*** |
| - | Reader2 | 1.00 | **<0.01*** | **<0.01*** | **<0.01*** | **0.01*** | **<0.01*** |
| Overall image quality | Reader1 | 1.00 | 0.67 | **0.02*** | 1.00 | **0.01*** | **<0.01*** |
| | Reader2 | 1.00 | 0.76 | **0.02*** | 1.00 | **0.01*** | **<0.01*** |

**Note:** Data are Bonferroni corrected *p*-values of Pairwise Wilcoxon signed rank test

* corrected *p*-value below 0.05 which means the pair has significant different score

CBD common bile duct, CHD common hepatic duct, cRHD central right hepatic duct, pRHD peripheral right hepatic duct, cLHD central left hepatic duct, pLHD peripheral left hepatic duct, pMPD proximal main pancreatic duct, mMPD middle main pancreatic duct, dMPD distal main pancreatic duct

### 3.2. Qualitative Analysis

The inter-reader agreement was almost perfect for the visibility scores of the CBD, cRHD, pRHD, cLHD, pLHD, pMPD, and dMPD (kappa=0.84, 0.91, 0.93, 0.89, 0.93, 0.82, and 0.85, respectively), and the artifact and overall image quality scores showed almost perfect agreement (kappa=0.88 and 0.99, respectively). Additionally, the visibility scores of the CHD, cystic duct, and mMPD showed substantial inter-reader agreement (kappa=0.71, 0.80, and 0.80, respectively). Therefore, the visibility, artifact, and overall image quality scores are shown in Table **3** and the pairwise comparison data of the MRCPs are presented in Tables **4** and **5**. Moreover, these data are also shown in Fig. (**S1**) which can be viewed in the supplement.

All qualitative scores significantly differed among the four MRCP sequences according to the Friedman test (all *p*-values were under 0.006). For pairwise comparison, all *p*-values of the Wilcoxon signed-rank test with Bonferroni correction were tabulated in Appendix **1**. The CBD visibility score was significantly higher for BH-CS than for BH-GRAPPA for both readers (reader 1: 4.55 *vs*. 4.16, $p < 0.01$; reader 2: 4.49 *vs*. 4.10, $p < 0.01$). The CHD visibility score was significantly higher for BH-CS than for BH-GRAPPA and RT-GRAPPA for both readers (reader 1: 4.57 *vs* 4.20 and 4.23, $p < 0.01$ and $p < 0.01$, respectively; reader 2: 4.41 *vs*. 3.97 and 4.05, $p < 0.01$ and $p = 0.03$, respectively). The cRHD visibility score was significantly higher for BH-CS than for BH-GRAPPA for both readers (reader 1: 3.99 *vs*. 3.53, $p < 0.01$; reader 2: 3.96 *vs*. 3.54, $p < 0.01$). The pRHD visibility score had no significant difference in the pairwise Wilcox signed-rank tests of the four MRCP sequences. The cLHD visibility score was significantly higher for BH-CS than for BH-GRAPPA for both readers (reader 1: 3.98 *vs*. 3.52, $p < 0.01$; reader 2: 3.90 *vs*. 3.38, $p < 0.01$). The pLHD visibility score was significantly lower for BH-GRAPPA than for RT-GRAPPA and RT-CS for both readers (reader 1: 2.22 *vs* 2.73 and 2.67, $p = 0.01$ and $p = 0.02$, respectively; reader 2: 2.23 *vs*. 2.74 and 2.66, $p = 0.02$ and $p = 0.04$, respectively). The cystic duct visibility score was significantly higher for BH-CS than for BH-GRAPPA for both readers (reader 1: 3.78 *vs*. 3.23, $p < 0.01$; reader 2: 3.61 *vs*. 3.16, $p = 0.02$). The pMPD visibility score did not show a consistently significant difference between the two readers. The mMPD visibility score was significantly higher for RT-CS than for BH-GRAPPA for both readers (reader 1: 3.59 *vs*. 3.03, $p < 0.01$; reader 2: 3.55 *vs*. 3.01, $p < 0.01$). The dMPD visibility score was significantly higher for RT-CS than for BH-GRAPPA for both readers (reader 1: 3.19 *vs*. 2.66, $p = 0.02$; reader 2: 3.11 *vs*. 2.58, $p < 0.01$).

The artifact score was significantly higher for BH-CS than for other three MRCP sequences (reader1: 2.64 *vs*. RT-GRAPPA 2.18, $p < 0.01$; *vs*. RT-CS 2.16, $p < 0.01$; *vs*. BH-GRAPPA 1.84, $p < 0.01$; reader2: 2.57 *vs*. RT-GRAPPA 2.20, $p < 0.01$; *vs*. RT-CS 2.18, $p < 0.01$; *vs*. BH-GRAPPA 1.86, $p < 0.01$), $p < 0.01$). BH-GRAPPA showed the lowest artifact score of the four MRCP sequences (reader1: *vs*. RT-GRAPPA $p < 0.01$; *vs*. RT-CS $p < 0.01$; reader2: *vs*. RT-GRAPPA $p < 0.01$; *vs*. RT-CS $p < 0.01$). RT-GRAPPA and RT-CS showed no significant difference in the artifact score (2.18 *vs*. 2.16, $p > 0.05$).

The overall image quality score was significantly lower for BH-GRAPPA than for all other MRCP sequences (reader1: 2.71 *vs*. RT-GRAPPA 3.13, $p = 0.02$; *vs*. RT-CS 3.21, $p < 0.01$; *vs*. BH-CS 3.40, $p < 0.01$; reader2: 2.71 *vs*. RT-GRAPPA 3.14, $p = 0.02$; *vs*. RT-CS 3.24, $p < 0.01$; *vs*. BH-CS 3.40, $p < 0.01$). There were no significant differences in overall image quality score between RT-GRAPPA and RT-CS, between RT-GRAPPA and BH-CS, and between RT-CS and BH-CS.

## 4. DISCUSSION

In the quantitative evaluation results, relative contrast (RC) values were significantly higher for CS-MRCPs regardless of patients breathing for GRAPPA-MRCPs in our study. In previous studies comparing the RCs of 3D-MRCP with parallel imaging only and CS-MRCP, the RC values tended to be smaller when CS was applied [4, 15, 19]. Additionally, a previous study showed that CS-MRCP had a higher RC than that for conventional MRCP [13]. However, in the current study, when CS was applied, the RC value was higher than that of GRAPPA alone. The difference in these results may be the result of differences in the CS algorithm between vendors and differences in MR parameters, such as the acceleration factor for parallel imaging or the under-sampling factor for CS.

In the qualitative analysis, BH-CS showed similar or superior scores in visibility, artifact, and overall image quality compared to those for the other MRCP sequences (Fig. **4**). These results may be due to a reduced impact of artifacts with a short acquisition time, and an increased contrast by the denoising effect of the CS algorithm [20]. These results are consistent with those of previous studies [4, 7, 13, 15, 21]. Especially for the artifact score, BH-CS showed significantly higher scores compared to those for all other MRCP sequences. Since the artifact score was evaluated according to the range of the area affected by the artifact, respiratory artifacts were likely to have the greatest impact. Therefore, BH-CS with the shortest acquisition time (16 seconds) was expected to show the best artifact score.

Blurring of fine details is associated with CS, possibly related to the denoising effect in CS reconstruction [4, 20], which may have lowered the visibility scores of the peripheral and pancreatic ducts. In addition, left hepatic ducts are more susceptible to cardiac motion due to their location. However, even for the pRHD, pLHD, and MPD, neither BH-CS nor RT-CS showed inferiority to GRAPPA MRCP sequences. Moreover, the overall image quality was assessed as non-diagnostic for only two of the 98 BH-CS images. Thus, vulnerability to fine details with CS-MRCP should not be a significant problem in clinical practice.

Fortunately, breath-holding for 16 seconds was possible for most of the patients in the current study. However, this could be difficult for patients with lung disease, mental disorders, or hearing loss in real clinical practice (Fig. **5**). According to our study results, RT-CS showed similar image quality to that of BH-CS. In addition, the acquisition time of RT-CS (ideally 1 min 51 sec) is much shorter than that of RT-GRAPPA (ideally 3 min 32 sec). Considering the image quality and acquisition time comprehensively, it would be reasonable to use RT-CS for non-cooperative patients who are unable to hold their breath.

Regarding BH-3D-MRCP, the acquisition was technically possible without applying CS, but the parameters had to be intensively adjusted to achieve single BH acquisition (thicker and fewer slices, and fewer excitation numbers than that in the other three sequences). Nevertheless, the final acquisition time was approximately 21 seconds, which could result in lower patient compliance, as compared to that with 16 seconds for BH-CS. Thus, the visibility, artifact, and overall image quality scores for BH-GRAPPA might be rendered lower than those for other MRCP sequences.

This study has several limitations. First, there may be selection bias, as some patients were excluded from the

visibility score analysis of each segment. However, since all 98 patients in the study underwent scanning with four MRCP sequences without a missing sequence, this would not be a significant statistical weakness in proving the superiority of BH-CS. Secondly, this study was a single-vendor study. There may be differences in results with scanners from other vendors because there are differences in the CS algorithm among vendors. Third, there is a limit to clinical application because diagnostic performance is not evaluated in this study. Moreover, since we only reviewed maximal intensity projection images, there is a possibility that the evaluation of image quality would be different if the source image was reviewed. However, in clinical practice, MRCP is primarily reviewed in MIP form, rather than as a source image; thus, the current comparison is more meaningful clinically. Finally, since the study design was retrospective in nature, there may have been unavoidable bias.

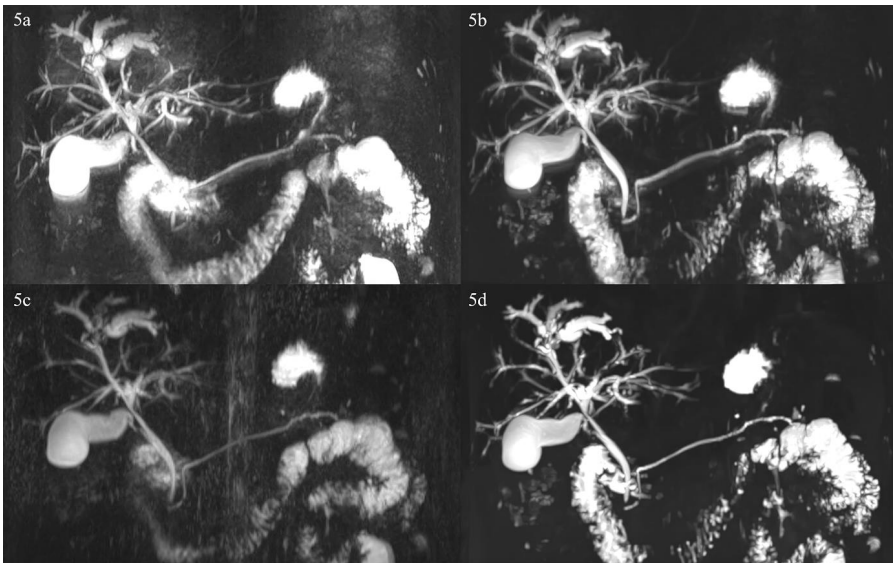


**Fig. (4).** A 67-year-old man underwent MRCP for an evaluation of intrahepatic duct dilatation.
The overall image quality scores of two readers were 4 for RT-GRAPPA (**4a**), 4 for RT-CS (**4b**), 4 for BH-GRAPPA (**4c**), and 5 for BH-CS (**4d**).
**Note**: *MRCP: magnetic resonance cholangiopancreatography, RT: respiratory-triggered; BH: breath hold, CS: compressed sensing, GRAPPA: generalized autocalibrating partially parallel acquisition.*

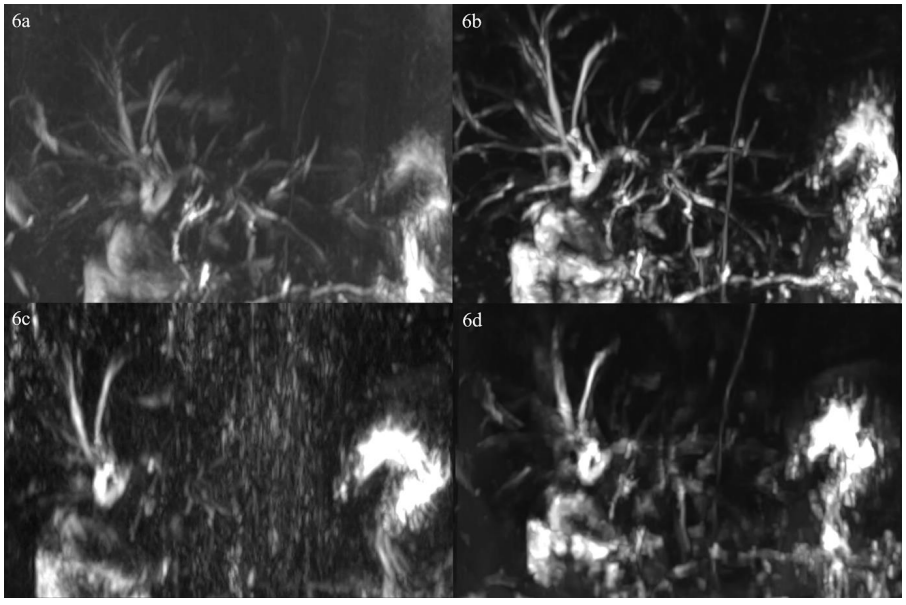


**Fig. (5).** A 70-year-old woman who had pylorus-preserving pancreaticoduodenectomy due to pancreatic head cancer underwent MRCP for a 6-month follow-up. She had poor cooperation for breath-holding. The overall image quality scores of the two readers were 3 for RT-GRAPPA (**5a**), 4 for RT-CS (**5b**), 1 for BH-GRAPPA (**5c**), and 2 for BH-CS (**5d**). BH sequences were severely affected by motion artifacts, while RT sequences showed relatively good image quality.
**Note**: *MRCP: magnetic resonance cholangiopancreatography, CBD: common bile duct, RT: respiratory-triggered; BH: breath hold, CS: compressed sensing, GRAPPA: generalized autocalibrating partially parallel acquisition.*

## CONCLUSION

In conclusion, BH-CS is clinically feasible and has comparable or better image quality compared to that for conventional MRCP, while reducing acquisition time. Using RT-CS may be more reasonable for patients with difficulty in breath holding.

## LIST OF ABBREVIATIONS

| | | |
|---|---|---|
| **RT** | = | Respiratory-triggered |
| **CS** | = | Compressed Sensing |
| **RC** | = | Relative Contrast |
| **PACE** | = | Prospective Acquisition Correction |

## ETHICS APPROVAL AND CONSENT TO PARTICIPATE

This retrospective study was approved by the Chung-Ang University Hospital, Chung-Ang University College of Medicine, (IRB No. 2107-025-19375).

## HUMAN AND ANIMAL RIGHTS

No animals were used for studies that are the basis of this research. All human procedures followed were in accordance with the guidelines of the Helsinki Declaration of 1975.

## CONSENT FOR PUBLICATION

The requirement of informed consent was waived.

## STANDARDS OF REPORTING

STROBE guidelines were followed.

## AVAILABILITY OF DATA AND MATERIALS

The data and supportive information is available within the article.

## FUNDING

None.

## CONFLICT OF INTEREST

The authors declare no conflicts of interest, financial or otherwise.

## ACKNOWLEDGEMENTS

Declared none.

## REFERENCES

[1] Griffin N, Charles-Edwards G, Grant LA. Magnetic resonance cholangiopancreatography: The ABC of MRCP. Insights Imaging 2012; 3(1): 11-21. [http://dx.doi.org/10.1007/s13244-011-0129-9] [PMID: 22695995]

[2] Taylor ACF, Little AF, Hennessy OF, Banting SW, Smith PJ, Desmond PV. Prospective assessment of magnetic resonance cholangiopancreatography for noninvasive imaging of the biliary tree. Gastrointest Endosc 2002; 55(1): 17-22. [http://dx.doi.org/10.1067/mge.2002.120324] [PMID: 11756908]

[3] Vidal BPC, Lahan-Martins D, Penachim TJ, Rodstein MAM, Cardia PP, Prando A. MR cholangiopancreatography: What every radiology resident must know. Radiographics 2020; 40(5): 1263-4. [http://dx.doi.org/10.1148/rg.2020200030] [PMID: 32870770]

[4] Seo N, Park MS, Han K, *et al.* Feasibility of 3D navigator-triggered magnetic resonance cholangiopancreatography with combined parallel imaging and compressed sensing reconstruction at 3T. J Magn Reson Imaging 2017; 46(5): 1289-97. [http://dx.doi.org/10.1002/jmri.25672] [PMID: 28295827]

[5] Lee JH, Lee SS, Kim JY, *et al.* Parallel imaging improves the image quality and duct visibility of breathhold two-dimensional thick-slab MR cholangiopancreatography. J Magn Reson Imaging 2014; 39(2): 269-75. [http://dx.doi.org/10.1002/jmri.24155] [PMID: 23596083]

[6] Yeh BM, Liu PS, Soto JA, Corvera CA, Hussain HK. MR imaging and CT of the biliary tract. Radiographics 2009; 29(6): 1669-88. [http://dx.doi.org/10.1148/rg.296095514] [PMID: 19959515]

[7] Yoon JH, Lee SM, Kang HJ, *et al.* Clinical feasibility of 3-Dimensional magnetic resonance cholangiopancreatography using compressed sensing. Invest Radiol 2017; 52(10): 612-9. [http://dx.doi.org/10.1097/RLI.0000000000000380] [PMID: 28448309]

[8] Bates DDB, LeBedis CA, Soto JA, Gupta A. Use of magnetic resonance in pancreaticobiliary emergencies. Magn Reson Imaging Clin N Am 2016; 24(2): 433-48. [http://dx.doi.org/10.1016/j.mric.2015.11.010] [PMID: 27150328]

[9] Feng L, Benkert T, Block KT, Sodickson DK, Otazo R, Chandarana H. Compressed sensing for body MRI. J Magn Reson Imaging 2017; 45(4): 966-87. [http://dx.doi.org/10.1002/jmri.25547] [PMID: 27981664]

[10] Jaspan ON, Fleysher R, Lipton ML. Compressed sensing MRI: A review of the clinical literature. Br J Radiol 2015; 88(1056): 20150487. [http://dx.doi.org/10.1259/bjr.20150487] [PMID: 26402216]

[11] Yoon JH, Nickel MD, Peeters JM, Lee JM. Rapid imaging: Recent advances in abdominal mri for reducing acquisition time and its clinical applications. Korean J Radiol 2019; 20(12): 1597-615. [http://dx.doi.org/10.3348/kjr.2018.0931] [PMID: 31854148]

[12] Ye JC. Compressed sensing MRI: A review from signal processing perspective. BMC Biomed Eng 2019; 1(1): 8. [http://dx.doi.org/10.1186/s42490-019-0006-z] [PMID: 32903346]

[13] Song JS, Kim SH, Kuehn B, Paek MY. Optimized breath-hold compressed-sensing 3D MR cholangiopancreatography at 3T: Image quality analysis and clinical feasibility assessment. Diagnostics 2020; 10(6): 376. [http://dx.doi.org/10.3390/diagnostics10060376] [PMID: 32517113]

[14] Kwon H, Reid S, Kim D, Lee S, Cho J, Oh J. Diagnosing common bile duct obstruction: Comparison of image quality and diagnostic performance of three-dimensional magnetic resonance cholangiopancreatography with and without compressed sensing. Abdom Radiol 2018; 43(9): 2255-61. [http://dx.doi.org/10.1007/s00261-017-1451-6] [PMID: 29302736]

[15] Kromrey ML, Funayama S, Tamada D, *et al.* Clinical evaluation of respiratory-triggered 3D MRCP with navigator echoes compared to breath-hold acquisition using compressed sensing and/or parallel imaging. Magn Reson Med Sci 2020; 19(4): 318-23. [http://dx.doi.org/10.2463/mrms.mp-2019-0122] [PMID: 31645536]

[16] Chandarana H, Doshi AM, Shanbhogue A, *et al.* Three-dimensional MR cholangiopancreatography in a breath hold with sparsity-based reconstruction of highly undersampled data. Radiology 2016; 280(2): 585-94. [http://dx.doi.org/10.1148/radiol.2016151935] [PMID: 26982678]

[17] Morita S, Ueno E, Suzuki K, *et al.* Navigator-triggered prospective acquisition correction (PACE) technique *vs*. conventional respiratory-triggered technique for free-breathing 3D MRCP: An initial prospective comparative study using healthy volunteers. J Magn Reson Imaging 2008; 28(3): 673-7. [http://dx.doi.org/10.1002/jmri.21485] [PMID: 18777550]

[18] Hosseinzadeh K, Furlan A, Almusa O. 2D thick-slab MR cholangiopancreatography: Does parallel imaging with sensitivity encoding improve image quality and duct visualization? AJR Am J Roentgenol 2008; 190(6): W327-34. [http://dx.doi.org/10.2214/AJR.07.2854] [PMID: 18492874]

[19] Nagata S, Goshima S, Noda Y, *et al.* Magnetic resonance cholangiopancreatography using optimized integrated combination with parallel imaging and compressed sensing technique. Abdom Radiol (NY) 2019; 44(5): 1766-72. [http://dx.doi.org/10.1007/s00261-018-01886-0] [PMID: 30659308]

[20] Worters PW, Sung K, Stevens KJ, Koch KM, Hargreaves BA. Compressed-Sensing multispectral imaging of the postoperative spine. J Magn Reson Imaging 2013; 37(1): 243-8. [http://dx.doi.org/10.1002/jmri.23750] [PMID: 22791572]

[21] Tokoro H, Yamada A, Suzuki T, *et al.* Usefulness of breath-hold compressed sensing accelerated three-dimensional magnetic resonance cholangiopancreatography (MRCP) added to respiratory-gating conventional MRCP. Eur J Radiol 2020; 122: 108765. [http://dx.doi.org/10.1016/j.ejrad.2019.108765] [PMID: 31830630]